Title
Calcium Binding Dramatically Stabilizes an Ancestral Crystallin Fold in Tunicate βγ-Crystallin

Journal
Biochemistry, 55(50)

ISSN
0006-2960

Authors
Kozlyuk, Natalia
Sengupta, Suvrajit
Bierma, Jan C
et al.

Publication Date
2016-12-20

DOI
10.1021/acs.biochem.6b00937

Peer reviewed

Published in final edited form as:

Biochemistry. 2016 December 20; 55(50): 6961–6968. doi:10.1021/acs.biochem.6b00937.

Calcium binding dramatically stabilizes an ancestral crystallin fold in tunicate $\beta\gamma$-crystallin

Natalia Kozlyuk[‡], **Suvrajit Sengupta**[‡], **Jan C. Bierma**[§], **Rachel W. Martin**[*,‡,§]

Department of Chemistry, University of California, Irvine, CA 92697-2025, USA, and Department of Molecular Biology and Biochemistry, University of California, Irvine, CA 92697-3900, USA

Abstract

The tunicate (*Ciona intestinalis*) $\beta\gamma$-crystallin represents an intermediate case between the calcium-binding proteins ancestral to the vertebrate $\beta\gamma$-crystallin fold and the vertebrate structural crystallins. Unlike the structural $\beta\gamma$-crystallins in the vertebrate eye lens, this $\beta\gamma$-crystallin strongly binds Ca^{2+}. Furthermore, Ca^{2+} binding greatly stabilizes the protein, an effect that has previously been observed in microbial $\beta\gamma$-crystallins but not in those of vertebrates. This relationship between binding and protein stabilization makes the tunicate $\beta\gamma$-crystallin an interesting model for studying the evolution of the human $\beta\gamma$-crystallin. We also compare and contrast the binding sites of tunicate $\beta\gamma$-crystallin with other $\beta\gamma$-crystallins in order to develop hypotheses as to the functional origin of the lack of the Ca^{2+} binding sites in the human crystallins.

Graphical Abstract

rwmartin@uci.edu.

[*]To whom correspondence should be addressed

[‡]Department of Chemistry, UC Irvine

[§]Department of Molecular Biology & Biochemistry, UC Irvine

Supporting Information Available

Supporting Information Available. The Supporting Information contains ITC figure of human γS-crystallin with Ca^{2+} and ^{15}N-^{1}H HSQC of human γS-crystallin in the absence and presence of Ca^{2+}, both showing the absence of Ca^{2+} binding. Also in the SI, are detailed methods on the sequential-binding fitting procedure of the tunicate $\beta\gamma$ crystallin ITC data using Mathematica. CD data were deposited to the CD database for both the apo and the holo forms under ID codes CD0005898000 and CD0005899000, respectively. The ^{1}H and ^{15}N chemical shifts for the apo and holo forms have been deposited in the BioMagRes Bank, under accession numbers 26860 and 26861, respectively.

This material is available free of charge via the Internet at http://pubs.acs.org/.

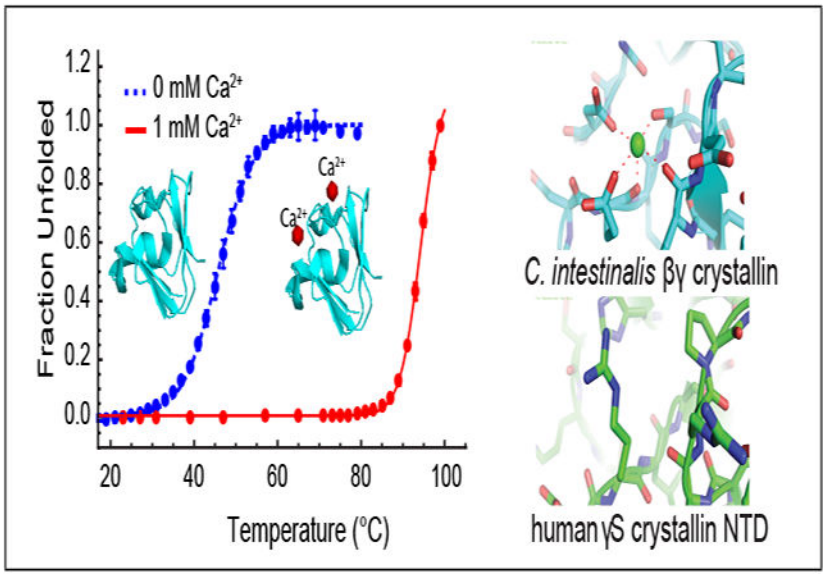

Keywords

$\beta\gamma$-crystallin; eye lens protein; protein evolution; protein stability; calcium-binding protein

The $\beta\gamma$-crystallin fold is an ancient structural motif found in diverse organisms from all three domains of life. In organisms without eyes, e.g. archaea (1), bacteria (2), tunicates (3), and sponges (4), $\beta\gamma$-crystallins serve as calcium-binding proteins. In vertebrates, they are primarily found in the eye lens, where they play an important role in controlling the refractive index gradient of this specialized tissue. The ubiquitous $\beta\gamma$-crystallins of the vertebrate lens are believed to have descended from an ancestral single-domain Ca^{2+}-binding crystallin by a process that included gene duplication resulting in two copies of the double Greek key domain per chain, as well as selection for high refractive index, concomitant with the loss of Ca^{2+}-binding functionality (5).

Phylogenetic analysis suggests that the $\beta\gamma$-crystallin superfamily, ubiquitous in vertebrates, evolved from a common ancestor also related to the sponge crystallin (4) and the spherulins of slime molds (6). The single-domain $\beta\gamma$-crystallin of the tunicate, *Ciona intestinalis*, (*Ci*-$\beta\gamma$-crystallin), appears to be representative of the single-domain ancestor of the vertebrate $\beta\gamma$-crystallin fold. However, the story of $\beta\gamma$-crystallin evolution is not a simple progression from simple to complex; the calcium-binding $\beta\gamma$-crystallin from the sponge *Geodia cydonium* has two domains linked by an interdomain interface; however the relative orientation of its its domains is reversed with respect to that of its vertebrate orthologs (7). Two-domain crystallins in microbes may have evolved via a different pathway after the divergence of single-domain ancestors, as evidenced by differences in the arrangement of the β-strands (8), as well as the absence of the Tyr-corner structures conserved in vertebrate members of the superfamily (9) and even the Trp corners thought to serve as critical folding nuclei (10).

Many microbial $\beta\gamma$-crystallins such as spherulin 3a from the slime mold *Physarum polycephalum* and protein S from the soil bacterium *Myxococcus xanthus* increase in stability upon binding Ca^{2+} (11, 12). The C-terminal domain of M-crystallin from the archaeon *Methanosarcina acetivorans* binds Ca^{2+} with only moderate to low affinity (K_d= 35 μM and 200 μM, for two different sites); however ion binding has a profound effect on the protein. Solution NMR structures reveal that both the apo and holo forms adopt the canonical $\beta\gamma$-crystallin fold, however in the holo form most of the β strands are longer, and a number of disorganized loops surrounding the metal binding site become much more ordered relative to the apo form. The protein stability also increases upon Ca^{2+} binding, with T_m values of 55 °C and 71 °C in the presence and absence of Ca^{2+}, respectively (13). This behavior is even more pronounced for some other microbial crystallins; the bacterial crystallin proteins of *Yersinia pestis* (10) and *Caulobacter crescentus* (14), and *Hahella chejuensis* (15) are fully or partly unstructured in the absence of calcium ions and adopt the characteristic double Greek key arrangement only upon binding Ca^{2+}.

In general, crystallins have been recruited from proteins of diverse function (16), leading to situations where it is difficult for multiple functions to be selected for simultaneously. This results in divergence in properties of the lens and non-lens proteins (17), or even of different isoforms within the lens (18). It has been suggested that the lack of Ca^{2+} binding is essential for vertebrate lens protein function. In a series of mammalian γB-crystallin variants, introducing features critical for the microbial crystallin Ca^{2+}-binding sites negatively impacted the protein stability, particularly in the presence of Ca^{2+} (5). The conclusions of this study suggest that loss of Ca^{2+}-binding ability is necessary prior to selection for high stability, due to Ca^{2+}-induced destabilization, particularly in single-domain proteins that lack the stabilizing influence of the interdomain interface. On the other hand, it has also been shown that bovine γB-crystallin binds Ca^{2+} ions, stabilizing its fold and playing a role in maintaining a homeostatic concentration of Ca^{2+} in the cell (19). Clearly, the relationship between Ca^{2+}-binding and $\beta\gamma$-crystallin function in the vertebrate eye lens is not straightforward. Here we investigate the tunicate *Ciona intestinalis* $\beta\gamma$-crystallin because of its unique evolutionary position between the microbial crystallins and the vertebrate lens proteins. Although the tunicate does not have an eye lens, these crystallins are found in organs rich in Ca^{2+}; namely the ocellus and otolith, which are responsible for sensing depth and light when the larva swims (16). We show that the tunicate $\beta\gamma$-crystallin binds Ca^{2+} with a high affinity, and that Ca^{2+}-binding greatly stabilizes the protein against both thermal and chemical denaturation. We also compare and contrast structures of the Ca^{2+} binding site of the tunicate $\beta\gamma$-crystallin with that of other $\beta\gamma$-crystallins in order to investigate the structural evolution of these proteins for the loss of Ca^{2+} binding.

Materials and Methods

Gene Construction, Protein Expression and Purification

A plasmid containing the *Ci*-$\beta\gamma$-crystallin gene, codon-optimized for *Escherichia coli*, was purchased from Blue Heron Biotechnology (Bothell, WA). Primers for cloning were purchased from Integrated DNA Technologies (Coralville, IA) and used to amplify the crystallin gene containing restriction sites for NcoI and XhoI. After PCR, the gene was

cloned into a pET28a(+) vector (Novagen, Darmstadt, Germany). *Ci-βγ*-crystallin was overexpressed in a Rosetta *Escherichia coli* cell line (DE3) using Studier's auto-induction protocol (20) for 20–24 hours at 25 °C. The cells were lysed, spun down and dialyzed overnight into a buffer containing 10 mM piperazine (pH 6), 10 mM NaCl, 0.05 % NaN_3. The protein was purified with an anion exchange column, eluting at ~ 200 mM NaCl in 10 mM piperazine, EDTA was added to the samples and size exclusion was performed, eluting into 10 mM Tris-HCl buffer (pH 7.1), 0.05 % NaN_3. SDS PAGE and ES MS were performed to verify the identity of the purified protein. For expression in minimal media, 50 mL of overnight *E. coli* culture containing the plasmid with *Ci-βγ*-crystallin gene was transfered 1 L LB media and grown to an OD_{550} of 1. The cultures were spun down and resuspended in 1 L of M9 minimal media with $^{15}NH_4Cl$. Afterwards, the cells were grown for two hours at 37 °C and induced with IPTG to a final concentration of 1 mM. The cells were then grown for an additional 20–25 hours at 25 °C and purified as stated above.

A plasmid containing wild-type human γS-crystallin, an N-terminal 6x His tag and a TEV protease cleavage sequence was amplified by PCR. The PCR product was cloned into a pET28a(+) vector (Novagen, Darmstadt, Germany). WT human γS-crystallin was overexpressed similar to *Ci-βγ*-crystallin for both ^{15}N labeled and natural abundance expressions and purified as stated in (21). After purification, EDTA was added and the protein samples were dialyzed in 10 mM Tris-HCl (pH 7.1), 0.05 % NaN_3.

All buffers were deionized using a Profinity IMAC uncharged resin (Biorad) for all subsequent experiments.

Circular Dichroism Spectroscopy

Purified tunicate *βγ*-crystallin was diluted to 0.075 mg/mL in 10 mM Tris-HCl buffer (pH7.1) for full circular dichroism spectra and in 10 mM HEPES buffer (pH 7.1) for unfolding experiments in the presence of either 1 mM EDTA (0 mM Ca^{2+}) or 1 mM $CaCl_2$. Measurements were performed using a J-810 spectropolarimeter (JASCO, Easton, MD) equipped with a thermal controller. Data were recorded between 260 nm and 190 nm using a 1 nm bandwidth and a 4 second response for full circular dichroism spectra.

Fluorescence Spectroscopy

The tryptophan fluorescence of purified tunicate *βγ*-crystallin was measured at concentrations of 0.1 mg/mL in 10 mM Tris-HCl buffer (pH 7.1), 0.05 % NaN_3 in the presence of either 1 mM EDTA or 1 mM $CaCl_2$ at room temperature. Data were acquired using a Varian Cary Eclipse fluorescence spectrophotometer with 10 nm excitation slits, and an excitation wavelength of 280 nm. Each spectrum is the average of three scans. The ratio of the signals at 360 nm, (corresponding to solvent-exposed tryptophans), and at 320 nm (buried tryptophans) were used to monitor protein unfolding during thermal and chemical denaturation experiments.

Thermal denaturation experiments were performed over a temperature range from 17–100 °C in two degree increments. As for the fluorescence spectra, the buffer used was 10 mM HEPES (pH 7.1), 0.05 % NaN_3. The sample temperatures were increased using a Quantum Northwest TC 1 temperature controller with a two minute equilibration at every

temperature point. Data were fit to a two-state equilibrium unfolding model in Mathematica to determine the thermal denaturation temperature (T_m) of each sample. Thermal denaturation experiments using intrinsic tryptophan fluorescence were also verified with DSC experiments in the absence and presence of 1 mM $CaCl_2$ in 10 mM MES buffer (pH 7.1) (Figure S1). Chemical denaturation experiments were performed with increasing concentrations of urea or guanidinium hydrochloride in 10 mM Tris (pH 7.1), 0.05 % NaN_3 in the presence of 1 mM EDTA or 1 mM $CaCl_2$. Samples were allowed to equilibrate for about 24 hours with guanidinium hydrochloride and for 48 hours with urea before fluorescence spectra were acquired. Each point in the spectrum is an average of 12 measurements. To determine the Gibbs free energy at room temperature and the dependence of ΔG on denaturant concentration (ΔG°_{w} and m, respectively), denaturation data were fit to either a two-state or a three-state model in Mathematica as performed by Morjana, et al (22) depending on the presence or absence of an intermediate.

Isothermal Titration Calorimetry

ITC measurements were performed using a MicroCal VP-ITC microcalorimeter. In all cases, the protein sample and $CaCl_2$ solutions were degassed prior to titration. A titration consisted of 3 μL injections of 5 mM $CaCl_2$ to a protein sample in 10 mM Tris-HCl (pH 7.1), 0.05 % NaN_3 every 300 seconds. Overall 60 titrations were carried out. To subtract the heat of dilution, 5 mM $CaCl_2$ was titrated into 10 mM Tris-HCl (pH 7.1), 0.05 % NaN_3 and the data were subtracted from the protein titration data. Two experimental runs were performed; one with 386 μM and one with 405 μM. The reported fit parameters (Table 1) are the means and the error bars are the standard deviations. ITC data were analyzed using Mathematica and the fitting functions are shown in the SI.

NMR experiments

Experiments were performed at 25 °C on a Varian ^{Unity}INOVA system operating at 800 MHz equipped with a $^{1}H/^{13}C/^{15}N$ 5 mm tri-axis PFG triple-resonance probe. ^{15}N-^{1}H HSQC experiments were acquired with 4 scans in the direct dimension and 64 scans in the indirect dimension at protein concentrations of 1.7 mM in the presence or absence of 10 mM $CaCl_2$.

Results

Unlike human γS-crystallin, *Ci-βγ* binds Ca^{2+} with strong affinity

Isothermal titration calorimetry (ITC) was performed in order to measure the Ca^{2+}-binding affintity of the tunicate βγ-crystallin (Figure 1). The data were best fit to a sequential binding model, and binding at both sites was enthalpically driven (Table 1). The binding constants for the two sites were found to be 5.0×10^{7} M^{-1} and 8.58×10^{6} M^{-1} with an overall dissociation constant of 0.048 μM $\left(K_d = \frac{1}{\sqrt{K_1 K_2}}\right)$, indicating a strong affinity for Ca^{2+}. The flatter portion of the curve is where sequential binding of Ca^{2+} occurs at the two sites. When the higher affinity site is saturated, the lower affinity site binds the rest of the Ca^{2+}, representative of the steep part of the curve. Other thermodynamic parameters were extrapolated from the best fit model and are tabulated in Table 1. In contrast, the ITC

thermogram of WT human γS-crystallin (Figure S2) showed no binding of Ca^{2+}, even at a 5 mM concentration, which is consistent with its lack of Ca^{2+} binding sites (5).

Ca^{2+} binding does not change the secondary structure of *Ci-βγ*-crystallin

Although the protein binds Ca^{2+} with relatively strong affinity, circular dichroism (CD) and fluorescence data do not indicate significant changes in protein structure upon addition of 1 mM Ca^{2+}, representing a 100:1 Ca^{2+}: protein stoichiometric ratio. The CD spectra in the presence and absence of Ca^{2+} are almost identical, indicating that there is very little change in the secondary structure of the protein. The strong minimum around 218 nm under both conditions (Figure 2a) is consistent with the protein remaining in a mostly β-sheet conformation. With the addition of 1 mM Ca^{2+}, the intrinsic tryptophan fluorescence intensity is slightly increased at its peak maximum compared to the fluorescence spectrum in the presence of 1 mM EDTA (Figure 2b), however the emission wavelength does not shift, suggesting that the environment of the two tryptophans remains mostly unchanged.

The resistance of *Ci-βγ*-crystallin to both thermal and chemical denaturation dramatically increases upon binding Ca^{2+}

Thermal denaturation experiments were performed using the intrinsic tryptophan fluorescence over a 17–100 °C temperature range. In globular proteins, the signals from the solvent-exposed and buried tryptophans appear at approximately 360 and 320 nm, respectively. In this case, the emission maxiumum of the folded protein appears at 332 nm. Here unfolding is monitored using the ratio of the 360/330 peak intensities, normalized to plot the fraction unfolded as a function of temperature (Figure 3). Ca^{2+} binding results in a dramatic increase in resistance to thermal denaturation. In the absence of Ca^{2+}, the protein begins to unfold at a temperature as low as 35 °C and fully denatures by about 70 °C, with a T_m of 45.8 °C. Upon addition of Ca^{2+}, the temperature at the onset of denaturation rises to about 83 °C, while T_m increases to 94.2 °C. Denaturation of both the apo and the holo forms of the protein were reversible upon cooling to the initial temperature.

Binding to Ca^{2+} also protected the *Ci-βγ*-crystallin against chemical denaturation by both GndHCl and urea. Protein unfolding was observed in the presence of both denaturants for the apo form and in GndHCl for the holo form. The emission maximum for the intrinsic tryptophan fluorescence shifts by about 30 nm with the addition of the maximum denaturant concentration (Figure S3). In the absence of Ca^{2+}, the protein begins to denature at concentrations of GndHCl as low as 0.25 M and keeps unfolding until about 3 M GndHCl has been added (Figure 4a) having a $[\text{denaturant}]_{1/2}$ of 1.75 M. In the presence of Ca^{2+}, GndHCl unfolding curves show gradual unfolding initiated again at 0.25 M, but the steeper unfolding is not initiated until 3 M GndHCl (Figure 4a). The same experiment for the holo form indicates the presence of an intermediate and the data were therefore fit to a three-state model with two transition points at $[\text{denaturant}]_{1/2}$ of 0.74 and 4.08 M. The overall ΔG°_{w} was found to be 5.08 kcal · mol^{-1} for the two unfolding transitions in the presence of Ca^{2+} as compared to 2.77 kcal · mol^{-1} in the absence of Ca^{2+}. Refolding experiments in the absence of Ca^{2+} were found to be reversible but in the presence of this divalent metal, the protein

only refolded back to its intermediate state instead of fully back to its native state. ΔG°_{w}, m, and $[\text{denaturant}]_{1/2}$ are tabulated in Table 2 for GndHCl.

Resistance to unfolding by urea is even more dramatically increased in the presence of Ca^{2+}. Ca^{2+} stabilizes *Ci*-$\beta\gamma$-crystallin against detectable unfolding even at very high urea concentrations approaching saturation. In the absence of Ca^{2+}, the protein begins to unfold starting at 0.25 M urea and continues to unfold until 5 M urea (Figure 4b). Compared with the GndHCl data for the apo from of the protein, the $[\text{denaturant}]_{1/2}$ was lower (1.26 M) indicating that the protein was not as stable in urea. Refolding experiments showed that the unfolding curve was reversible upon lowering the denaturant concentration.

Discussion

Ci-$\beta\gamma$-crystallin strongly binds Ca^{2+}, and binding of this divalent metal ion dramatically increases the stability of the protein to denaturation by heat, GndHCl, and urea. The addition of Ca^{2+} stabilized the protein structure, where the midpoint of the transition temperature increased by almost 50 °C, from 45.8 °C to 94.2 °C. Previous studies have shown that the binding of Ca^{2+} stabilizes the structures of many non-lens $\beta\gamma$-crystallins such as Protein S and Spherulin 3a, which are microbial proteins produced during stress (10). The T_m of the apo form is comparable to those of the microbial $\beta\gamma$-crystallins, (i.e. T_m of Flavollin is 47.3 °C, Rhodollin is 45.2 °C, Clostrillin is 44.6 °C (23)), however the increase in the transition temperature of the holo form is much higher than what has previously been observed for other proteins. This observation can perhaps be attributed to the tighter binding affinity of *Ci*-$\beta\gamma$-crystallin for Ca^{2+}.

Ci-$\beta\gamma$-crystallin bound Ca^{2+} at both of its sites with a higher affinity than previously observed for many non-mammalian $\beta\gamma$-crystallins (i.e. overall K_d for M-crystallin is 32 μM, Clostrillin is 4 μM and for rhodollin crystallin is 370 μM). The data were fit to a sequential binding model in which one site has a higher K_d than the other; K_{d1} is 0.020 μM and K_{d2} is 0.12 μM. Despite the high Ca^{2+} affinity of this protein, CD and intrinsic tryptophan fluorescence spectra did not show dramatic changes in secondary structure, even upon addition of 100:1 stoichiometric ratio of Ca^{2+} to protein. This result is consistent with other studies showing that the binding of Ca^{2+} does not induce major conformational changes in protein S and spherulin 3a (19).

The microbial $\beta\gamma$-crystallins act as Ca^{2+} storage proteins, while most of the vertebrate $\beta\gamma$-crystallins appear to lack functional Ca^{2+} binding sites. Questions still remain about the reason the human $\beta\gamma$-crystallin evolved to lose its metal ion binding sites, and whether the high stability of the mammalian proteins, even without binding Ca^{2+}, represents a necessary tradeoff in function. Disturbance in Ca^{2+} homeostasis is one way that cataract can develop in the eye lens (24). The Ca^{2+} sites remain functional in some vertebrate $\beta\gamma$-crystallins (e.g. bovine γB), potentially contributing to the regulation of Ca^{2+} homeostasis in the mammalian lens. In Figure 5, we compare the sequences of M-crystallin, bovine γ-crystallin, clostrillin microbial crystallin, human γS-crystallin, *Ci*-$\beta\gamma$-crystallin and the *Geodia cydonium* sponge crystallin, for which the binding site is highly similar to that of the *Ci*-$\beta\gamma$-crystallin. This comparison provides insight into the loss of Ca^{2+} binding sites in some vertebrate

crystallins. Despite their very similar folds, the sequences of the mammalian $\beta\gamma$-crystallin family have diverged from the signature Ca^{2+} binding sequence of NDXXSS (25) in such a way that the Ca^{2+} binding sites have a lower binding affinity for Ca^{2+} due to the substitution of some functionally important residues in the signature sequence. Comparing the $\beta\gamma$-crystallins from different organisms shows that there are only seven positions that are strictly conserved, and nine that are functionally conserved. Of the residues involved in calcium binding, only one is in a strictly conserved site and another in a functionally conserved site. By comparing sequences of $\beta\gamma$-crystallins with functional calcium binding sites to those that are unable to bind Ca^{2+}, it can be seen that some structural rearrangement has taken place during the selection of these proteins to fulfill their role in the lens (Figure 5). This structural rearrangement appears to eliminate the necessary Ca^{2+} binding contacts, eliminating some sidechain carbonyls and reorienting other backbone carbonyls that were involved in binding. Additionally, two positively charged residues at or near the binding site have been added, leading possibility of forming salt bridges with the negatively charged residues, which would both disrupt the interactions with Ca^{2+} and generate an electrostatic repulsion between the residue and the calcium ion. It is likely that other subtle and complicated nonlinear binding effects play a role in the loss of Ca^{2+} binding that has occurred during the evolution of vertebrate crystallins. More experimental data on related proteins is needed to fully characterize these effects.

Although the bovine γ-crystallin is able to bind Ca^{2+}, it does so with weaker affinity (90 μM) as compared to the tunicate crystallin. The residues involved in Ca^{2+} binding are similar to that of the tunicate (Glu 46, Arg 47, Asp 73, Ser 74) (19), but there is also a positively charged residue in the binding pocket which might be responsible for the weaker Ca^{2+} affinity. Overall, the Ca^{2+} binding affinity decreases for $\beta\gamma$-crystallins, and in many cases Ca^{2+} binding destabilizes the proteins. The presence of the additional domain (CTD) in the cow and human crystallins has been hypothesized to increase the protein's stability, compensating for the evolutionary decrease in Ca^{2+} binding affinity (5).

Examination of the crystal structure of the holo form (PDBID 2BV2) (3) reveals that negatively charged residues such as glutamic and aspartic acid participate in binding the divalent metal ions, along with serine. Specifically, Glu 7, Ile 33, Ser 35 and Asp 75 make up one of the two Ca^{2+} binding sites and Asp 32, Asp 48, Glu 76 and Ser 78 make up the other (3) (Figure 6). Although CD and fluorescence do not indicate large changes in protein secondary structure, solution-state NMR data (chemical shifts measured via ^{15}N-^{1}H HSQC) do show peak shifts for residues involved in binding Ca^{2+} upon addition of 10 mM $CaCl_2$, indicating more subtle, local conformational changes responsible for stabilizing the protein against denaturation. The HSQC spectra for the apo forms are overlaid in Figure 7a. The ^{1}H and ^{15}N chemical shifts for the apo and holo forms have been deposited in the BioMagRes Bank, under accession numbers 26860 and 26861, respectively. Chemical shift perturbation weighted averages upon addition of Ca^{2+} were measured using the chemical shift perturbation equation: $\Delta\delta_{avg} = \sqrt{\frac{\left(\Delta\delta_N/5\right)^2 + \left(\Delta\delta_H\right)^2}{2}}$. Chemical shift perturbations upon addition of Ca^{2+} are plotted in Figure 7b, with thresholds for large (> 0.2 ppm) and moderate (0.06 – 0.2 ppm) perturbations shown. Residues for which the shift was less than 0.06 ppm

were classified as unperturbed. These perturbations are shown in the context of the structure in Figure 7c. Examination of these data in the context of the protein structure suggest that the slight change in the fluorescence spectra upon addition of Ca^{2+} (Figure 2b) may be caused by a change in the local environment of Trp 70. Similarly, in a previous study, several residues were perturbed in the NMR spectrum upon addition of Ca^{2+} to M-crystallin, another case where Ca^{2+}-binding stabilized the protein (13). In contrast, when Ca^{2+} was added to WT human γS-crystallin, no significant peak shifts were observed (Supplementary Figure S4), consistent with the lack of Ca^{2+} suggested by the ITC data.

As for thermal denaturation, results from the chemical denaturation experiments also showed that the addition of Ca^{2+} greatly stabilized *Ci*-$\beta\gamma$-crystallin, possibly due to the tighter packing of the protein in the presence of the divalent ions. When GndHCl was used as the denaturant, the protein was more stable in the holo form as compared to the apo form. Unfolding of the holo form, but not the apo form, proceeded via an intermediate. The $[GndHCl]_{1/2}$ was 1.8 M in the apo form and 0.74/4.1 M for the two unfolding transitions respectively, in the holo form. The $[GndHCl]_{1/2}$ of the apo form were similar to those of many other $\beta\gamma$-crystallins such as those of the microbial crystallins, however, the $[GndHCl]_{1/2}$ values for the holo form exceeded that which have been previously observed for single domain $\beta\gamma$-crystallins (i.e. protein S has a $[GndHCl]_{1/2}$ of 1.7 M, however, it only increases to 1.9 M in the presence of Ca^{2+} in contrast to this tunicate crystallin) (26, 27). The overall free energy of unfolding was also consistent with the $[denaturant]_{1/2}$ where the protein was more stable and more resistant to denaturation in the presence of Ca^{2+} (5.08 in the holo form versus 2.77 kcal $\cdot$ mol^{-1} in the apo form). This observation is also consistent with the result that the T_m was higher for the tunicate crystallin in the presence of Ca^{2+} than for these microbial crystallins.

When urea was added to the tunicate protein in the presence of Ca^{2+}, the protein became completely resistant to unfolding. Vertebrate γB-crystallin has also been shown to resist denaturation by urea at pH 7 due to strong interactions between its two domains (12). In the apo form, the $[urea]_{1/2}$ was 1.26 M, which is relatively unstable relative to other similar crystallins. The large difference in urea denaturation susceptibility between the apo and holo forms, coupled with the smaller difference in GndHCl sensitivity suggests some hypotheses about the mechanism of stabilization.GndHCl is an ionic denaturant that could shield the favorable electrostatic interactions between the positive Ca^{2+} and the negative residues at the binding sites, reducing the Ca^{2+}-protein interaction and allowing a loosening of the fold. On the other hand, urea denaturation has been hypothesized to occur either via direct or indirect mechanisms. The direct mechanism occurs when urea hydrogen bonds to the polar groups of the proteins, which unfolds the protein and exposes the hydrophobic residues to solvation with the water molecules and urea. The indirect mechanism occurs when urea disrupts the water structure around the protein which weakens the hydrophobic effect and exposes those non polar residues to the solvent (28). The ionic character of GndHCl may explain the lower resistance against this type of chemical denaturation in the holo form, as it is competing with the Ca^{2+} for the residues involved in the Ca^{2+} binding sites. Its ionic character could also be responsible for stabilizing an intermediate along the unfolding pathway of the holo form, however, this is not seen in the apo form. Urea, on the other hand, has little effect on electrostatics and primarily binds to the protein during denaturation via polar interactions.

Thus, no denaturation is observed in the holo form of *Ci-βγ*-crystallin even at high concentrations, however, the lower $[denaturant]_{1/2}$ value for the apo form of the protein with urea as compared to GndHCl makes it seem that urea is a stronger denaturant for this protein in the absence of the stabilizing metal ions. Follow-up NMR experiments at varying concentrations presence of urea and GndHCl will be performed to further elucidate the differences in how the protein is chemically unfolded by these two denaturants.

Conclusion

The *Ciona intestinalis βγ* crystallin, an ancestor of the vertebrate lens crystallins, binds Ca^{2+} with high affinity. In contrast, human γS-crystallin lacks many of the key residues involved in metal ion binding, and does not bind Ca^{2+}. In the tunicate protein, Ca^{2+} binding dramatically increases the protein's thermal and chemical stability, to a larger degree than has been previously observed for single domain crystallins. This result provides a basis for future studies of the evolution of vertebrate lens proteins from ancestral Ca^{2+}-storage proteins.

Supplementary Material

Refer to Web version on PubMed Central for supplementary material.

Acknowledgement

The authors thank Dr. Dmitry Fishman for excellent management of the UCI Optical Spectroscopy Facility, Dr. Andor Kiss for helpful discussions and Dr. Muneera Beach for assistance with the DSC experiments.

Funding

This work was supported by NSF DMR-1410415 and NIH 1R01EY021514 to R.W.M.

Abbreviations

NMR	nuclear magnetic resonance
UV	ultraviolet

References

1. Barnwal RP, Jobby MK, Sharma Y, and Chary KVR (2006) NMR assignment of M-crystallin: a novel Ca^{2+} binding protein of the *βγ*-crystallin superfamily from *Methanosarcina acetivorans*. J. Biomol. NMR 36, 32–32. [PubMed: 16607466]
2. Wistow G, Summers L, and Blundell T (1985) *Myxococcus xanthus* spore coat protein S may have a similar structure to vertebrate lens *βγ*-crystallins. Nature 315, 771–773. [PubMed: 3925350]
3. Shimeld SM, Purkiss AG, Dirks RP, Bateman OA, Slingsby C, and Lubsen NH (2005) Urochordate *βγ*-crystallin and the evolutionary origin of the vertebrate eye lens. Curr. Biol 15, 1684–1689. [PubMed: 16169492]
4. Krasko A, Müller IM, and Müller WEG (1997) Evolutionary relationships of the metazoan *βγ*-crystallins, including that from the marine sponge *Geodia cydonium*. Proc. Royal Soc. B 264, 1077–1084.
5. Suman SK, Mishra A, Yeramala L, Das Rastogi I, and Sharma Y (2013) Disability for function: loss of Ca^{2+}-binding is obligatory for fitness of mammalian *βγ*-crystallins. Biochemistry 52, 9047–9058. [PubMed: 24251594]

6. Rosinke B, Renner C, Mayr EM, Jaenicke R, and Holak TA (1997) Ca^{2+}-loaded spherulin 3a from *Physarum polycephalum* adopts the prototype gamma-crystallin fold in aqueous solution. J. Mol. Biol 271, 645–655. [PubMed: 9281431]
7. Vergara A, Grassi M, Sica F, Pizzo E, D'Alessio G, Mazzarella L, and Merlino A (2013) A novel interdomain interface in crystallins: structural characterization of the $\beta\gamma$-crystallin from *Geodia cydonium* at 0.99 Å resolution. Acta Crystallographica Section D: Biological Crystallography D69, 960–967.
8. Clout NJ, Kretschmar M, Jaenicke R, and Slingsby C (2001) Crystal structure of the calcium-loaded spherulin 3a dimer sheds light on the evolution of the eye lens $\beta\gamma$-crystallin domain fold. Structure 9, 115–124. [PubMed: 11250196]
9. Hamill JH, Cota E, Chothia C, and Clarke J (2000) Conservation of folding and stability within a protein family: the tyrosine corner as an evolutionary cul-de-sac. J. Mol. Biol 295, 641–649. [PubMed: 10623553]
10. Jobby MK, and Sharma Y (2005) Calcium-binding crystallins from *Yersinia pestis* - Characterization of two single -crystallin domains of a putative exported protein. J. of Biol. Chem 280, 1209–1216. [PubMed: 15536081]
11. Kretschmar M, Mayr E-N, and Jaenicke R (1999) Kinetic and thermodynamic stabilization of the $\beta\gamma$-crystallin homolog spherulin 3a from *Physarum polycephalum* by calcium binding. J. Mol. Biol 289, 701–705. [PubMed: 10369756]
12. Wenk M, and Jaenicke R (1999) Calorimetric analysis of the Ca^{2+}-binding *beta*γ-crystallin homolog protein S from *Myxococcus xanthus*: intrinsic stability and mutual stabilization of domains. J. Mol. Biol 293, 117–124. [PubMed: 10512720]
13. Barnwal R, Jobby MK, Devi KM, Sharma Y, and Chary KV (2009) Solution structure and calcium-binding properties of M-crystallin, a primordial $\beta\gamma$-crystallin from archaea. J. Mol. Biol 386, 675–689. [PubMed: 19138688]
14. Jobby MK, and Sharma Y (2007) Caulollins from *Caulobacter crescentus*, a pair of partially unstructured proteins of $\beta\gamma$-crystallin superfamily, gain structure upon binding calcium. Biochemistry 46,, 12298–12307. [PubMed: 17915944]
15. Srivastava AK, and Chary KVR (2011) Conformational heterogeneity and dynamics in a -crystallin from *Hahella chejuensis*. Biophys. Chem 157, 7–15. [PubMed: 21549498]
16. Slingsby C, Winstow GJ, and Clark AR (2013) Evolution of crystallins for a role in the vertebrate eye lens. Protein Science 22, 367–380. [PubMed: 23389822]
17. Wistow G (1993) Lens crystallins: gene recruitment and evolutionary dynamism. Trends in Biochemical Sciences 18, 301–306. [PubMed: 8236445]
18. Kingsley CN, Bierma J, Pham V, and Martin R (2014) The γS-crystallin proteins from the Antarctic Nototheniid Toothfish: a model system for investigating differential resistance to chemical and thermal denaturation. J. Phys. Chem. B 118, 13544–13553. [PubMed: 25372016]
19. Rajini B, Shridas P, Sundari CS, Muralidhar D, Chandani S, Thomas F, and Sharma Y (2001) Calcium binding properties of gamma crystallin: Calcium ion binds at the greek key $\beta\gamma$-crystallin fold. J. Biol. Chem 276, 38464–38471. [PubMed: 11502736]
20. Studier FW (2005) Protein production by auto-induction in high-density shaking cultures. Protein expression and purification 41, 207–234. [PubMed: 15915565]
21. Brubaker WD, and Martin RW (2011) 1H, 13C, and 15N assignments of wild-type human γS-crystallin and its cataract-related variant γS-G18V. Biomolec. NMR Assign. 6, 63–67.
22. Morjana NA, McKeone BJ, and F., G. H. (1993) Guanidine hydrochloride stabilization of a partially unfolded intermediate during the reversible denaturation of protein disulfide isomerase. Proc. Natl. Acad. Sci. USA 90, 2107–2111. [PubMed: 8460117]
23. Aravind P, Mishra A, Suman SK, Jobby MK, Sankaranarayanan R, and Sharma Y (2009) The $\beta\gamma$-crystallin superfamily contains a universal motif for binding calcium. Biochemistry 48, 12180–12190. [PubMed: 19921810]
24. Duncan G, and Jacob T (1984) Calcium and the physiology of cataract. Ciba Foundation Symposium 106, 132–152. [PubMed: 6096095]
25. Srivastava SS, Mishra A, Krishnan B, and Sharma Y (2014) Ca^{2+}-binding Motif of $\beta\gamma$-Crystallins. J. Biol. Chem 289, 10958–10966. [PubMed: 24567326]

26. Suman SK, Mishra A, Ravindra D, Yeramala L, and Sharma Y (2011) Evolutionary remodeling of $\beta\gamma$-crystallins for domain stability at cost of Ca^{2+} binding. J. Biol. Chem 286, 43891–43901. [PubMed: 21949186]

27. Giancola C, Pizzo E, Di Maro A, Cubellis MV, and D'Alessio G (2005) Preparation and characterization of geodin. FEBS Journal 272, 1023–1035. [PubMed: 15691335]

28. Bennion B, and Daggett V (2003) The molecular basis for the chemical denaturation of proteins by urea. Proc. Natl. Acad. Sci. USA 100, 5142–5147. [PubMed: 12702764]

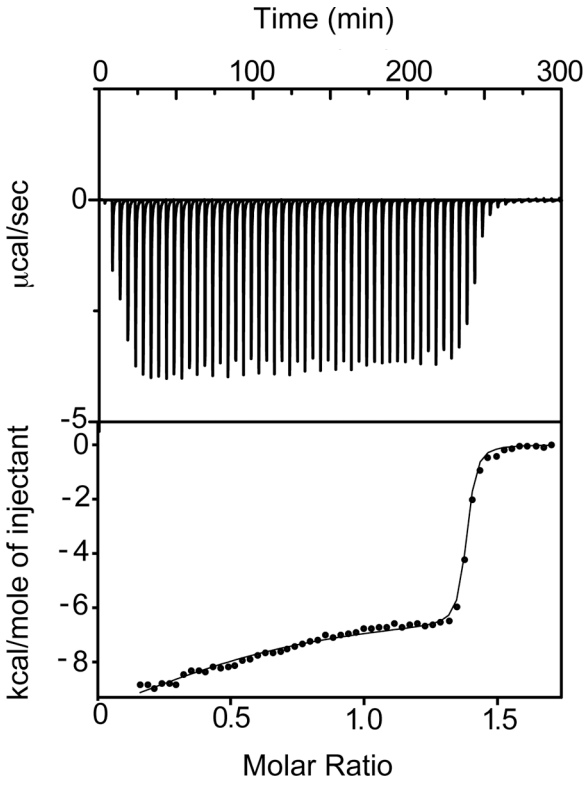

Figure 1:

Thermogram demonstrating the binding of Ca^{2+} to tunicate $\beta\gamma$-crystallin. Ca^{2+} (5 mM) was titrated into 386 μM protein sample in 10 mM Tris-HCl (pH 7.1) and the curve was best fit to a sequential binding model.

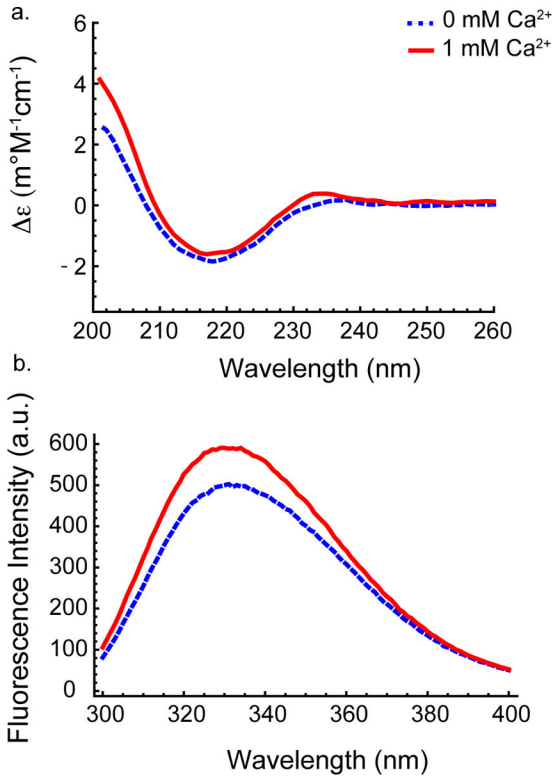

Figure 2:

(a) The CD spectra of both the apo (blue dashed line) and holo (red solid line) forms of tunicate $\beta\gamma$-crystallin display strong minima at 218 nm, indicating primarily β-sheet secondary structure that does not significantly change upon the addition of Ca^{2+}.(b) Similarly, the intrinsic tryptophan fluorescence signal displays only a slight increase in intensity as a result of Ca^{2+} binding. The wavelength of the emission maximum does not shift, indicating that the environment of the Trp residues remains mostly unchanged.

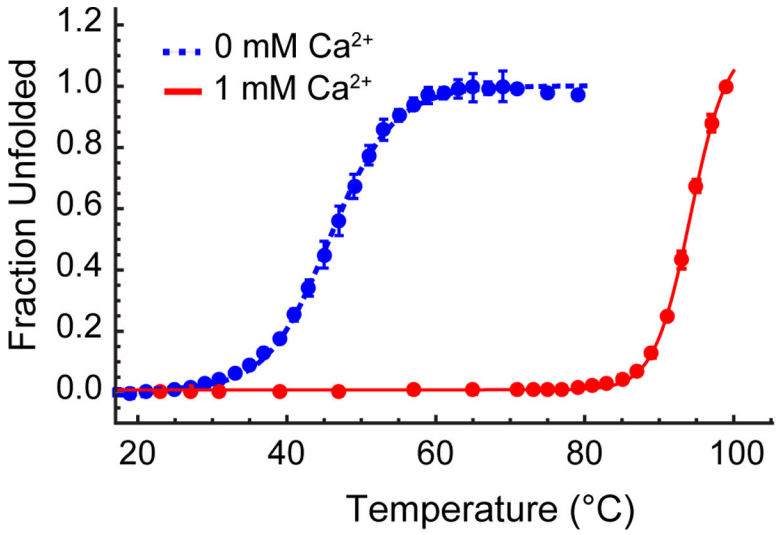

Figure 3:

Thermal denaturation curves showing the thermal stability of the protein measured over a range of 17–100 °C. The holo form of the protein shows an increase in thermal stability compared with the apo form. The T_m increases from 45.8 °C to 94.2 °C upon addition of Ca^{2+}. Open circles indicate reversibility of the experiment.

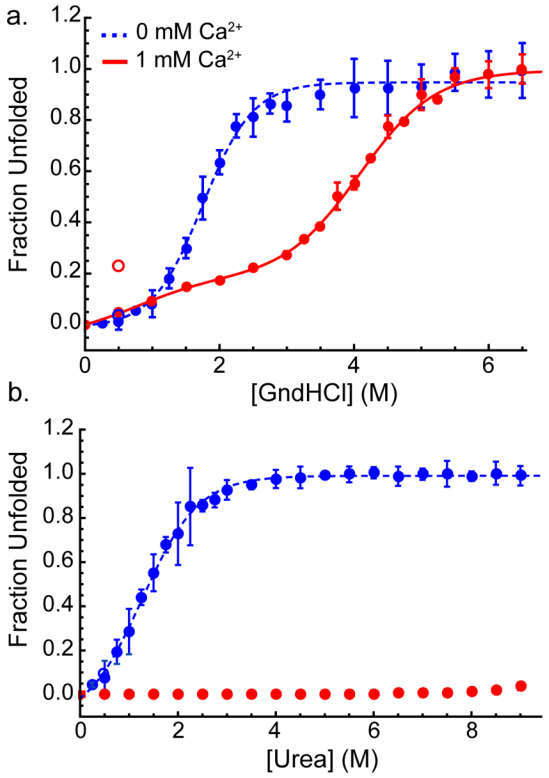

Figure 4:

The *Ci-βγ*-crystallin is resistant to chemical denaturation with (a) GndHCl and (b) urea upon addition of Ca^{2+}. Open circles indicate the reversibility of the experiment. Denaturation of the apo form is fully reversible in both denaturing conditions, while the holo form refolds to the intermediate state in the GndHCl denaturing conditions. The holo form does not unfold in urea, even at 9 M.

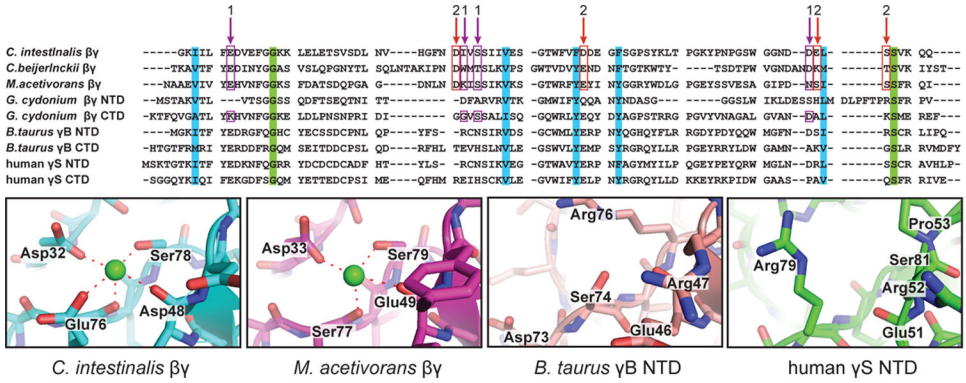

Figure 5:

(Top) Sequence alignment of $\beta\gamma$-crystalllins from *C. intestinalis*, *C. beijerinckii*, *M. acetivorans*, *G. cydonium*, *B. taurus*, and *H. sapiens*. Residues highlighted in green are strictly conserved, while residues highlighted in cyan are functionally conserved. Boxes enclose residues involved in calcium binding as determined by polar contacts made in the structure. Arrows indicate the calcium binding residues of sites 1 and 2. (Bottom) View of calcium binding site 2 in *C. intestinalis* $\beta\gamma$, *M. acetivorans* $\beta\gamma$, *B. taurus* γ-crystallin and human γS-crystallin.

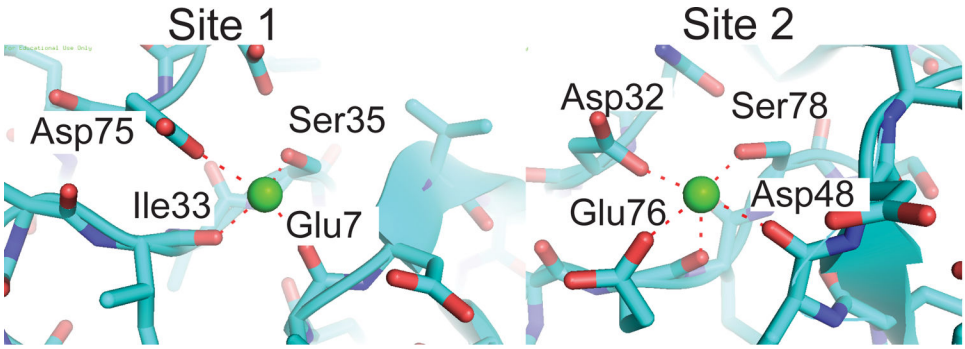

Figure 6:

Residues involved in the calcium binding sites of the tunicate $\beta\gamma$-crystallin, observed in the X-ray crystal structure PDBID 2BV2 (3)

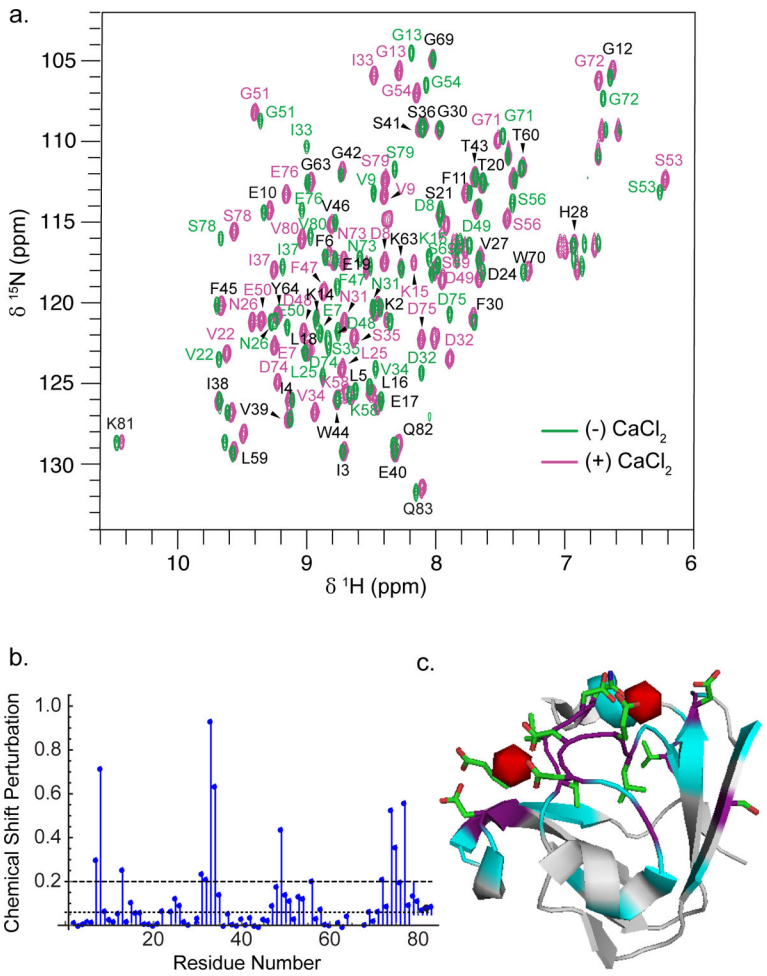

Figure 7:

a. ^{15}N-^{1}H HSQC spectra of the tunicate $\beta\gamma$-crystallin in the absence (green) and presence (magenta) of 10 mM $CaCl_2$. Residues that have the same chemical shift under both conditions are labeled in black. b. Average chemical shift perturbation plot as a function of residue number, with thresholds for large (> 0.2 ppm) and moderate (0.06–0.2ppm). Residues for which the shift is < 0.06 ppm upon addition of $CaCl_2$ are classified as unperturbed. c. The same CSP data represented on the X-ray crystal structure. The backbone corresponding to amide NHs for which the chemical shift perturbation is large are shown in purple, while amides that are slightly perturbed are in cyan and those of unperturbed residues are shown in gray. The two calcium ions are represented in red, while the side chains of the Ca^{2+}-binding residues are highlighted in green.

Table 1:

Thermodynamic parameters for binding of Ca^{2+} to *Ci-βγ*-crystallin.

	K **(M^{-1})**	**ΔH (kcal/mol)**	**ΔS (cal/mol·K)**	**ΔG (kcal/mol)**
Site 1	$5.0 \times 10^7 \pm 5.8 \times 10^4$	−9.9±0.21	3.7	−11
Site 2	$8.6 \times 10^6 \pm 5.0 \times 10^5$	−6.9±0.29	8.4	−9.4

Table 2:

Thermodynamic parameters for guanidinium hydrochloride denaturation

	$[denaturant]_{1/2}$ (M)	ΔG°_{w} (kcal/mol)	*m* (kcal/mol·M^{-1})
GndHCl (apo)	1.75	2.8 ± 0.095	1.6 ± 0.17
GndHCl (holo N → I)	0.74	0.77 ± 0.72	1.0 ± 0.59
GndHCl (holo I → U)	4.08	4.3 ± 0.37	1.1 ± 0.087